J. Membrane Biol. 189, 93–104 (2002)
DOI: 10.1007/s00232-002-1006-8

The Journal of
Membrane
Biology

Modeling Light-induced Currents in the Eye of *Chlamydomonas reinhardtii*

D. Gradmann[1], S. Ehlenbeck[2], P. Hegemann[2]

[1]Abteilung Biophysik der Pflanze, Albrecht-von-Haller-Institut für Pflanzenwissenschaften der Universität, Untere Karspüle 2, D-37073 Göttingen, Germany

[2]Institut für Biochemie, Universität Regensburg, D-93092 Regensburg, Germany

Received: 27 February 2002/Revised: 20 May 2002

Abstract. Rhodopsin-mediated electrical events in green algae have been recorded in the past from the eyes of numerous micro-algae like *Haematococcus pluvialis*, *Chlamydomonas reinhardtii* and *Volvox carteri*. However, the electrical data gathered by suction-pipette techniques could be interpreted in qualitative terms only. Here we present two models that allow a quantitative analysis of such results: First, an electrical analog circuit for the cell in suction pipette configuration is established. Applying this model to experimental data from unilluminated cells of *C. reinhardtii* yields a membrane conductance of about 3 Sm^{-2}. Furthermore, an analog circuit allows the determination of the photocurrent fraction that is recorded under experimental conditions. Second, a reaction scheme of a rhodopsin-type photocycle with an early Ca^{2+} conductance and a later H^+ conductance is presented. The combination of both models provides good fits to light-induced currents recorded from *C. reinhardtii*. Finally, it allowed the calculation of the impact of each model parameter on the time courses of observable photocurrent and of inferred transmembrane voltage. The reduction of the flash-to-peak times at increasing light intensities are explained by superposition of two kinetically distinct rhodopsins and by assuming that the Ca^{2+}-conducting state decays faster at more positive membrane voltages.

Key words: Analog circuit — Channelrhodopsin — Photocycle — Proton conductance — Reaction kinetics — Rhodopsin

Correspondence to: D. Gradmann; email: dgradma@gwdg.de

Introduction

Light-induced, rhodopsin-mediated currents have been recorded from green algae like *Haematococcus pluvialis* (Litvin, Sineshchekov & Sineshchekov, 1978), *Chlamydomonas reinhardtii* (Harz & Hegemann, 1991), and *Volvox carteri* (Braun & Hegemann, 1999), when the cells had been partially sucked into the measuring pipette of a pA-meter. The light-induced currents recorded from the eyespot region were similar in all species and the basic observations can be summarized as follows: Upon excitation of the eye by a saturating light flash of about 0.5 mE m^{-2} and 10 μsec duration, a first light-induced current, I_{P1}, starts after a delay of only about 50 μsec. I_{P1}, passes a peak of up to −50 pA about 1 msec after the flash, and decays with a time constant between 1 and 10 msec (Sineshchekov, Litvin & Keszethely, 1990; Holland et al., 1996; Ehlenbeck et al., 2002). I_{P1} is assumed to be predominantly carried by Ca^{2+} with a half-saturating external Ca^{2+} concentration of about 10 μM. The properties of I_{P1} in green algae are in several respects similar to light-induced currents, I_P, in invertebrate eyes but the delay of I_{P1} in algae is much shorter than in all invertebrates. This difference led to the idea that I_{P1} is only limited by photoconversion of the rhodopsin (Sineshchekov et al., 1990; Harz, Nonnengäßer & Hegemann, 1992; Holland et al.,1996; Ehlenbeck et al., 2002) and does not employ an extra, transmitter-mediated conductance, as suggested by Calenberg et al. (1998).

In experiments carried out on *C. reinhardtii* at pH 4.5 or below, a slower current transient, I_{P2}, is superimposed on I_{P1} (Ehlenbeck et al., 2002). The I_{P2} transient passes a maximum of up to about 10 pA at >10 msec after the flash. Because of its dependence on $[H^+]_o$, I_{P2} has been suggested to be carried by H^+ (Ehlenbeck et al., 2002). The suggestion of an in-

trinsic, passive proton conductance of a chlamyopsin has recently been verified for one of the recently identified microbial-type rhodopsins, after expression in *Xenopus* oocytes. Accordingly, this rhodopsin was named channelrhodopsin-l (Nagel et al., 2002).

A detailed analysis of the photocurrents shows that both I_{P1} and I_{P2} are comprised of a low-light saturating component *a* and a high-light saturating component *b* (Ehlenbeck et al., 2002). The currents I_{P1a} and I_{P2a} saturate in flash experiments when only 1% of the responsible rhodopsin is bleached. The ion specificities of *a* and *b* are slightly different (Sineshchekov et al., 1990, Holland et al., 1996). The *a* and *b* current components have different susceptibility to retinal analogs when pigment-depleted cells are reconstituted with such components (Govorunova et al., 2001). These results support the earlier-drawn conclusion that two rhodopsin species mediate phobic responses and phototaxis (Zacks et al., 1993; Sineshchekov & Govorunova, 2001; Ehlenbeck, 2002). Delay and flash-to-peak times are much larger for the *a* component than for the *b* component (Braun & Hegemann, 1999; Ehlenbeck et al., 2002).

The photocurrents I_{P1} and I_{P2} as recorded in the suction-pipette configuration reflect only a fraction of the true photoreceptor currents. This fraction depends on the shape of the pipette, on the fraction of the cell sucked into the pipette, and, certainly, on the ionic conditions inside and outside the pipette (Harz et al., 1992; Holland et al., 1996). Therefore, amplitudes and time courses of these currents could be discussed in the past on a qualitative level only. For a quantitative analysis, direct measurements of the current I and the membrane voltage V by intracellular recordings or patch clamp recordings from the eye area would be more informative. Unfortunately, such data are not available due to the unfavorable properties of the plasma membrane even of cell wall-less cells, and due to the small cytoplasmic volume (Nichols & Rikmenspoel, 1978).

Nevertheless, the present study aims for a quantitative interpretation of the light-induced current transients I_{P1} and I_{P2} by employing two physical models that account for the electrical circuitry of the suction-pipette configuration and for the formation of electrically conducting states within the photocycle of rhodopsin. If not stated otherwise, the present study refers to the high-intensity component *b* only. The kinetics of the more complex, low-intensity component *a* include an amplification mechanism and will be subject of a separate study.

In its basic form, the combined model does not account for the familiar observation that the flash-to-peak time becomes shorter upon increasing intensities of the stimulating light flash. For low light intensities, this feature has been explained, already, by superposition of the effects of the two systems *a* and *b*

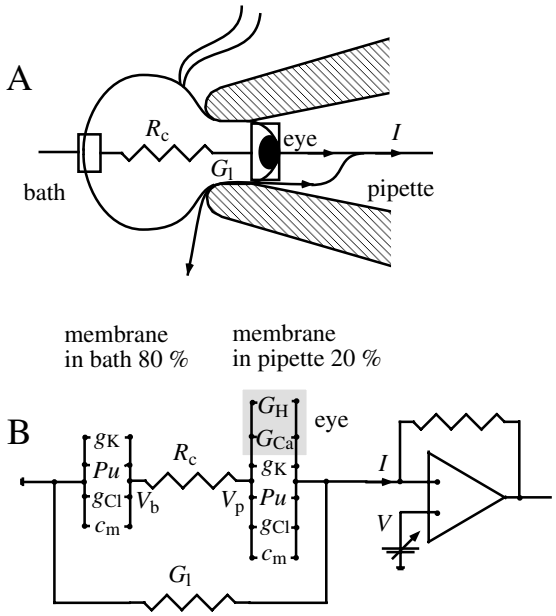

Fig. 1. Electrical model of a cell with eye, held in the measuring pipette of a pA-meter (patch-clamp amplifier). (*A*) Physical configuration. (*B*) Equivalent circuit. R_c, resistance of cell interior, found to be small enough to be ignored here; G_l, leak conductance between cell and glass; can be ignored at zero command voltage (V at amplifier, on the right in part *B*). g_K, K^+ conductance of dark membrane, not used; g_{Cl} (g_m), passive Cl^- transport through the membrane in the dark; *Pu*, electrogenic pump, acting mainly as a source of V-independent outward current in physiological V range; c_m, standard membrane capacity V_b and V_p, membrane voltages in the bath and pipette compartment, respectively; G_{Ca} and G_H in shaded area (eye), tentative conductances of chlamyrhodopsin for Ca^{2+} and H^+, respectively.

(Ehlenbeck et al., 2002). And for high intensities, this relationship is simulated by the model, with the additional assumption that the Ca^{2+}-conducting state in the photocycle of system *b* decays faster at more positive membrane voltages. This assumption is consistent with previous reports on voltage-dependent kinetics of rhodopsins (Nagel et al., 1998; Geibel et al., 2001); and the predictions agree with the kinetic effects of external $[K^+]$ (Nonnengäßer et al., 1996) and of cell size (Braun & Hegemann, 1999).

Altogether, the present approach comprises several steps of modeling: (*i*) The electrical properties of the unilluminated membrane; (*ii*) the photocycle of a single chlamyrhodopsin with an early conducting state for Ca^{2+} and a later one for H^+; and (*iii*) the concept of voltage-sensitive steps in the photocycle to explain the observation of faster responses upon stronger light stimuli. As a consequence, the explicit description of the phenomena cannot be presented by one algebraic master equation, but by an algorithm that comprises several steps of calculations, including iterative procedures. Introduction and application of this algorithm are the aim of this study.

Table 1. Reference parameters of models

Parameter and comments	Symbol	Magnitude	Unit
Background:			
Surface area of the cell	A	5×10^{-10}	m^2
Portion of cell surface in pipette,	a_{pip}	0.2	
Chloride membrane conductance	g_{Cl}	0.33	Sm^{-2} mM^{-1}
Cytoplasmic [Cl^-]	$[Cl]_i$	10	mM
External [Cl^-]	$[Cl]_o$	10	mM
Pump reference voltage, $\Delta G_{ATP}/F$	E_P	−480	mV
Maximum amount of H^+ pump current	$I_{Pu,mx}$	5000	Am^{-2} mM^{-1}
Internal H^+ concentration, rounded estimate	$[H^+]_i$	10^{-4}	mM
External H^+ concentrations, rounded estimates	$[H^+]_o$	10^{-4}, 10^{-2}	mM
Membrane capacitance, standard	c_m	10^{-2}	Fm^{-2}
Eye, non-kinetic:			
Total number of rhodopsin molecules in the eye	Rh_t	10^{-4}	
Maximum Ca^{2+} current through one rhodopsin	$I_{Ca,mx}$	10^{-14}	A
Reference photon exposure, 50% saturating	$Q_{1/2}$	6×10^{-5}	Em^{-2}
H^+ conductance of one rhodopsin molecule	g_H	10^{-12}	S mM^{-1}
Eye, rate constants for transitions			
L to M, formation of $G(Ca^{2+})$	k_{LM}	2912	sec^{-1}
M to N, decay of $G(Ca^{2+})$	k_{MN}	506	sec^{-1}
N to O, formation of $G(H^+)$	k_{NO}	98	sec^{-1}
O to P, decay of $G(H^+)$	k_{OP}	19	sec^{-1}

Model Description

Electrical Configuration

Figure 1 illustrates the experimental situation. The essential parameters of this model are listed in Table 1 with short descriptions. We assume that a cell with a surface A is sucked with the membrane portion a_{pip} into the orifice of a suction pipette that is electrically connected with a pA-meter. In Fig. 1, the eye is assumed to reside in the portion of the membrane that is exposed to the pipette solution. If the eye were located in the bath compartment, the recorded photoreceptor currents would be qualitatively identical with those of the chosen configuration. Only the sign inverts and the detected portion of the current is smaller (Harz et al., 1992). So the "eyespot out" configuration does not require another explicit discussion.

Dark Conditions

Before light-induced events can be discussed, the electrical properties of the plasma membrane have to be defined for dark conditions. For the present purpose, we assume the plasma membrane without eye to be electrically characterized by three entities:

First, a passive conductance g_m, which comprises electrodiffusion through the resting membrane. The most familiar membrane conductance is a nonlinear g_K, due to electrodiffusion of K^+. Because $[K^+]_o \ll [K^+]_i$, however, g_K is small at a resting voltage, V_r, of about −150 mV (Malhotra & Glass 1995) in the first place. Secondly, K^+ currents in plants are usually recorded far from equilibrium when the K^+ pathways become active. In contrast, close to the equilibrium, E_K, K^+ channels in plants are usually inactive. So there are good reasons to assign g_m to diffusion of a non-K^+ ion. A good candidate is Cl^-. Assigning electrodiffusion of Cl^- to g_m has the additional benefit of approximate linearity because about 10 mM external [Cl^-] are frequently used in suction pipette experiments (e.g., Ehlenbeck et al., 2002), and similar internal [Cl^-] can be expected as well. So we assumed an *ohmic* membrane conductance reflecting electrodiffusion of Cl. Our choice, $g_{Cl} = g_m \neq g_K$, is not compelling but reasonable and does not affect the main conclusions about the eye drawn in this study. Nevertheless, for the sake of completeness, g_K is marked in Fig. 1, because our simulation program does allow to account for g_K as well. Since this option has not been used in the present context, g_K is not listed in Table 1. Experimental determination of the resting conductance g_m is a prime subject of this study.

The second element is an electrogenic ion pump, *Pu*, which acts as an active source of outward current, i_{Pu}. With known values of the resting voltage V_r (Malhotra & Glass, 1995) and g_m (to be determined below), the pump current is $i_{Pu} = V_r \cdot g_m$ in this simplistic model.

The third element is a standard membrane capacitance, c_m, which affects the temporal characteristics of electrical events in the range of msec and faster.

Since the membrane voltage, V_m, is crucial in all electrical membrane processes but is not directly accessible in suction-pipette experiments, we used indirect estimates of V_m and its changes during I_{P1} and I_{P2}. These estimates of V_m are intermediate results in the course of calculating the photocurrents by the models described.

For the determination of the linear membrane conductance $g_m = g_{Cl}$ at $[Cl^-]_i = [Cl^-]_o = 10$ mM, an equivalent circuit (*see* Fig. 2) with four resistances has been assumed to account for the gross resistance $R = (R_1 + R_2)(R_3 + R_4)/(R_1 + R_2 + R_3 + R_4)$ between bath and pipette, where the four resistances R_1 to R_4 have the following meaning. R_1: seal resistance between membrane and glass at the tip of the pipette; $R_2 = r_2 \cdot l$: longitudinal resistance of the cylindrical (length l) interface (with length-related resistivity r_2) between glass and membrane in the pipette; $R_3 = r_m \cdot A_b$: resistance of the membrane portion in the bath with the (area-related) membrane resistivity r_m and the area $A_b = \pi d^2$, where d is the diameter of the spherical cell portion in the bath; $R_4 = r_m \cdot A_p$: resistance of the membrane area $A_p = \pi l \delta$, with an inner diameter $\delta = 2.5$ μm of the cylindrical pipette tip (ignoring the small contribution of the inner cross section of the tip to A_p).

The parameters d and l have been varied by progressive suction of the cells into the pipette at constant δ; the distances d, l, and δ have been read from microscopical images (1 mm of the image

corresponding to 0.56 μm in the object plane). $R = V/I$ has been determined by measuring the transcellular current I at a small (1 mV) voltage V between pipette and bath. The measurements on four cells and the corresponding system parameters R_1, r_2, and $g_m = 1/r_m$, determined by a least-square fitting routine are listed in Table 2. Thus, the area-related membrane resistance, r_m, of the plasmalemma in individual cells of *C. reinhardtii* is about 0.3 Ω m^2 and the leak conductance $G_l = 1/(R_1 + R_2)$ about 10 nS (100 MΩ seal resistance).

According to our assumptions, $g_m = 1/r_m \approx 3.3$ S m^{-2} corresponds to a Cl^- conductance, g_{Cl}, of about 0.33 S m^{-2} mM^{-1} (Table 1) and the voltage of passive diffusion is $V_d = E_{Cl} = 0$ mV. With the only experimental estimate of $V_r \approx -150$ mV available in *C. reinhardtii* (Malhotra & Glass, 1995) and a voltage-independent pump current i_{Pu}, this current is determined by $i_{Pu} = V_r g_m \approx -0.5$ A · m^{-2}, corresponding to a concentration-related pump current of 5000 A · m^{-2} · mM^{-1} at $pH_i = pH_o = 7$. More precisely, the steady-state electrical properties of an electrogenic H^+ ATPase can be described by

$$i_{Pu} = i_{Pu,mx} \frac{[H^+]_i - [H^+]_o \exp(u_{ATP} - u)}{1 + \exp(u_{ATP} - u)} \quad (1)$$

with equal amounts of saturating pump currents, $i_{Pu,mx}$, at large positive and negative voltage displacements from equilibrium, and symmetric reference concentrations ($[H^+]_i = [H^+]_o = 1$ mM); $u = VF/(RT)$ is the normalized membrane voltage where V is the membrane voltage, and R, T, and F have their usual thermodynamic meanings; $u_{ATP} = \Delta G_{ATP}/(RT)$ corresponds to an equilibrium voltage $E_{Pu} = \Delta G_{ATP}/F \approx -480$ mV of the pump at $[H^+]_i = [H^+]_o$. Equation (1) is derived from the general current-voltage relationships of electrogenic pumps (Hansen et al. 1981).

The third electrical element of the unilluminated membrane, $c_m \approx 10$ mF · m^{-2}, is common to biological membranes. Together with g_m, it is expected to have significant smoothing effects on V changes in the temporal range of $\tau_m = c_m/g_m \approx 10$ msec and faster.

The currents through the elements g_m, *Pu*, and c_m, which are assumed to be uniformly distributed over the total membrane area, have been calculated by multiplication of the area-related currents by the membrane areas $A_p = A \cdot a_{pip}$ in the pipette and in the bath, $A_b = A(1 - a_{pip})$, respectively.

R_c in Fig. 1*B* represents the resistance of the cell interior between the membrane portions in the bath and in the pipette. In a first approach, R_c (= 500 kΩ for a 5-μm cube with a typical cytoplasmic resistivity of 1 Ω m) can be neglected compared with the membrane resistances (some 10 MΩ, *see* below) in series. In case of a more accurate approach, V_p across the membrane in the pipette and V_b across the membrane in the bath can differ when R_c is significant and when the two membrane portions are electrically asymmetric, e.g., by the presence of the eye in only one compartment, or by application of a transcellular, electrochemical gradient.

Light-induced Conductances in the Eye

The eye in Fig. 1 is represented by the light-induced conductances for Ca^{2+} and for H^+. These conductances have to be assumed to be nonlinear. In analogy to Eq. (1) we write for the Ca^{2+} currents

$$i_{Ca} = i_{Ca,mx} \cdot R_M \cdot \frac{[Ca^{2+}]_i - [Ca^{2+}]_o e^{-2u}}{1 + e^{-2u}} \quad (2)$$

where $i_{Ca,mx}$ is the maximum Ca^{2+} current through one rhodopsin molecule at 1 mM $[Ca^{2+}]$, and R_M is the number of rhodopsin molecules in the Ca^{2+}-conducting state *M*. Because of $[Ca^{2+}]_i \ll [Ca^{2+}]_o$, and $[Ca^{2+}]_o = 1$ mM in our experiments, only inward Ca^{2+} currents are considered here, which are $i_{Ca} = i_{Ca,mx} \cdot R_M \cdot 1$ mM, i.e., numerically simply the product of $i_{Ca,mx}$ (5.5 fA per rhodopsin molecule) and R_M.

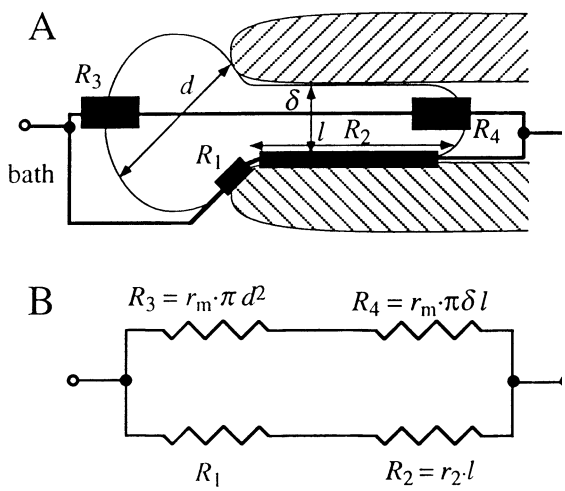

Fig. 2. Scheme and definitions of experimental configuration (*A*) and electrical equivalent circuit (*B*) for experimental determination of the membrane resistivity, $r_m = 1/g_m$, of cells, partly sucked into measuring pipette (*compare* Fig. 1). R_1, seal resistance between pipette tip and membrane; R_2, longitudinal resistance between glass and cylindric membrane portion in pipette; R_3, resistance of membrane area in bath; R_4, resistance of membrane area in pipette; d, diameter of spherical cell portion in bath; δ and l, diameter and length of cylindrical cell portion in pipette.

Previously, Harz et al. (1992) and Holland et al. (1996) have proposed a direct coupling between rhodopsin and the photoreceptor channel in *C. reinhardtii*. For the first qualitative considerations we followed this model for explaining the high-light saturating components of the photoreceptor current, I_{P1b} and I_{P2b} (Ehlenbeck et al., 2002). Now this model is extended for a quantitative description of the same currents. With 10^4 rhodopsin molecules in the cell (Beckmann & Hegemann, 1991) and a maximum inward current of −100 pA, an individual rhodopsin molecule in the Ca^{2+}-conducting state can pass 10 fA.

To describe the $I_H(V)$ relationship, a constant-field relationship has been taken as a first approach since the steady-state $I(V)$ of channelrhodopsin-1 (Nagel et al., 2002) do not show limitations imposed by V or $[H^+]$. Hence,

$$I_H(V) = V \cdot g_H \cdot \frac{[H^+]_i - [H^+]_o e^{-u}}{1 - e^{-u}} \quad (3)$$

where g_H is the H^+ conductance of a rhodopsin molecule in its H^+ conducting *O*-state (Fig. 3) at theoretical reference conditions ($[H^+]_i = [H^+]_o = 1$ mM).

Because of these nonlinear $I(V)$ relationships, the transmembrane voltage, V, has been calculated by an iterative procedure. Starting with a large voltage interval of about ≈ ±500 mV, very negative V will cause inward currents both in the pipette and in the bath compartment; correspondingly, large positive voltages cause outward currents. In the asymmetric configuration of an illuminated eye in the pipette compartment, we narrow down the voltage interval iteratively until a voltage is found where the inward current through the membrane in the pipette compartment equals the outward current through the membrane in the bath compartment. This voltage must be the desired membrane voltage, because it is the only one at which electroneutrality in the cell is maintained. The actual procedure accounts also for the possibility that the transmembrane voltage, V_p, in the pipette compartment differs

Table 2. Measured and calculated resistances used for the determination of the membrane conductance, g_m.

Cell	Trial	d (μm)	l (μm)	R (MΩ)		R_1 (MΩ)	r_2 (MΩ μm^{-1})	g_m (Sm^{-2})
				measured	calculated			
1	a	8.4	5.6	182	179	26	44	5.0
	b	7.8	10.1	182	196			
	c	5.6	19.6	263	244			
2	a	8.4	1.1	137	136	123	17	3.0
	b	7.8	2.8	152	154			
	c	6.7	11.2	200	199			
3	a	8.4	1.7	128	126	114	10	2.0
	b	7.8	5.6	143	150			
	c	6.7	11.2	189	178			
	d	5.6	16.8	208	211			
4	a	8.4	3.9	182	183	35	52	4.3
	b	7.2	9.0	217	225			
	c	6.7	14.0	244	238			
	Means ± SD					79 ± 42	31 ± 20	3.6 ± 1.3

Cells were sucked to various depths into the measuring pipette and the resistance determined after application of a voltage pulse; for definitions and explanations, *see* Fig. 2 and paragraph 5 of Dark Conditions in the Introduction.

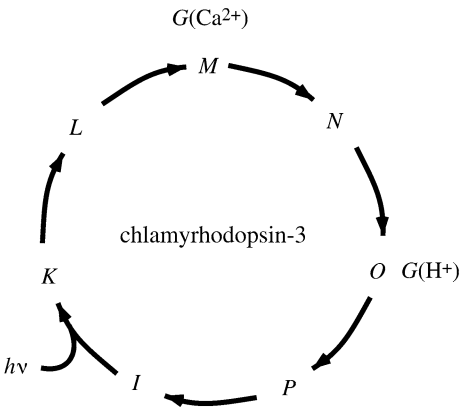

Fig. 3. Preliminary reaction cycle of chlamyrhodopsin *b*. *I*, ground state; *K*, primary state excited by light, *hν*; *L*, early intermediate, responsible for delay of < 50 μsec, not analyzed here; *M*, Ca^{2+}-conducting intermediate; *N*, nonconducting intermediate; *O*, H^+-conducting intermediate; *P*, intermediate(s) responsible for slow recovery of R_1 compared with decay of *O*.

from V_b in the bath compartment, i.e., when the resistance of the cell interior, R_c (*see* Fig. 1) is not ignored. In this case, the procedure yields both, V_p, and V_b ($= V_p + I_c \cdot R_c$), as well as the transcellular current $I_c = I_p = I_b$ of the serial arrangement.

A leak conductance G_l between pipette and bath has to be considered because the contact between glass and membrane in the suction configuration is not perfect with intact cells. A leak conductance $G_l \approx 10$ nS between glass and membrane has been obtained in the course of the determination of g_m (*see* column R_1 in Table 2). However, during the recordings of I_P, the voltage between bath and pipette was zero, and no background current through G_l had to be taken into account, therefore.

Hence, all parameters of the equivalent circuit in Fig. 1 are defined. Those that enter the analysis below are listed in Table 1. Because of the nonlinearities in the system, the iterative determination of V is not very robust. Frequently, convergence was only achieved after an *ad hoc* adjustment of the start interval of V.

Figure 3 shows a reaction cycle of the algal rhodopsin as used for the earlier qualitative analysis of Ehlenbeck et al. (2002). This reaction cycle comprises seven states and seven transitions of chlamyrhodopsin Rh_b, in alphabetical order starting with the inactive, resting state R_I. In this scheme, the states *M* and *O* represent the states for Ca^{2+} and H^+ conductance, respectively. R_I is the ground state (dark form); R_K marks the photoproduct and the first photocycle intermediate, which is formed from R_I with the rate constant $k_{IK} = k^0_{IK} \cdot Q$ where k^0_{IK} is k_{IK} at a standardized reference photon exposure, e.g., $Q_{1/2}$ for 50% bleaching, corresponding to about 60 μE m^{-2} typical for many rhodopsins (e.g., Ehlenbeck et al., 2002). The transition from R_I to R_K is supposed to be very fast compared with the following reaction steps. The next intermediate, R_L, is necessary to account for the short but measurable delay of I_{P1} (<50 μsec; Holland et al., 1996). I_{P1} is assigned to the state R_M, the tentative Ca^{2+}-conducting state, $G(Ca^{2+})$. Since in the present analysis, the delay is not treated explicitly, our kinetic calculations start with a certain amount, $p_L \cdot R_{tot}$, of rhodopsin molecules in the state R_L, where p_L is the portion of R_L of the total number, R_{tot}, of rhodopsin molecules. In our case, when the light flash and k_{KL} are below the temporal resolution, the initial portion $p_L = Q/(Q_{1/2} + Q)$ simply reflects saturation ($p_L \to 1$) for high Q, and half saturation ($p_L = 0.5$) at reference photon exposure of $Q = Q_{1/2}$. The nonconducting state *N* between the Ca^{2+} conductance *M* and the H^+ conductance *O* accounts for the typical notch in the current records between I_{P1} and I_{P2}. Finally, the last state, R_P, prior to the resting state R_I reflects the finding that more time than the decay of I_{P2} is required for a second high-intensity flash to cause full responses of I_{P1} and I_{P2}, i.e., to regenerate 100% of R_I. For the sake of simplicity, this recovery is not treated here explicitly either. Hence, for the present analysis only four states (*L*, *M*, N, and *O*) are considered explicitly with their corresponding transition probabilities k_{LM}, k_{MN}, k_{NO}, and k_{OP}.

For simplification of the formal treatment of this series of reactions, we use only the first index to identify the rate constants, e.g., $k_L = k_{LM}$ and define

$$L \overset{k_{LM}}{\to} M \overset{k_{MN}}{\to} N \overset{k_{NO}}{\to} O \overset{k_{OP}}{\to} = p_L \overset{k_L}{\to} p_M \overset{k_M}{\to} p_N \overset{k_N}{\to} p_O \overset{k_O}{\to}. \quad (4)$$

The time courses of the occupancies $p_i(t)$ for $j = L$ to *O*, will follow the form of the sum of exponentials

Table 3. Amplitude coefficients, p_{ij} ($i = L...O$, $j = 1...4$), of exponentials in time courses of occupancies p_i (t) in equation 7, for start conditions: $p_L = 1$, $p_{i>L} = 0$; first index, state; second index, exponential component.

$p_{L1} = \frac{Q}{Q_{1/2}+Q}$	$p_{L2} = 0$	$p_{L3} = 0$	$p_{L4} = 0$
$p_{M1} = p_{L1} \cdot \frac{k_L}{k_M - k_L}$	$p_{M2} = -p_{M1}$	$p_{M3} = 0$	$p_{M2} = 0$
$p_{N1} = p_{L1} \cdot \frac{k_M}{k_N - k_L} \cdot \frac{k_L}{k_M - k_L}$	$p_{N2} = p_{M2} \cdot \frac{k_M}{k_N - k_M}$	$p_{N3} = -p_{N1} - p_{N2}$	$p_{N4} = 0$
$p_{O1} = p_{L1} \cdot \frac{k_N}{k_O - k_L} \cdot \frac{k_M}{k_N - k_L} \cdot \frac{k_L}{k_M - k_L}$	$p_{O2} = p_{M2} \cdot \frac{k_N}{k_O - k_M} \cdot \frac{k_M}{k_N - k_M}$	$p_{O3} = p_{N3} \cdot \frac{k_N}{k_O - k_N}$	$p_{O4} = -p_{O1} - p_{O2} - p_{O3}$

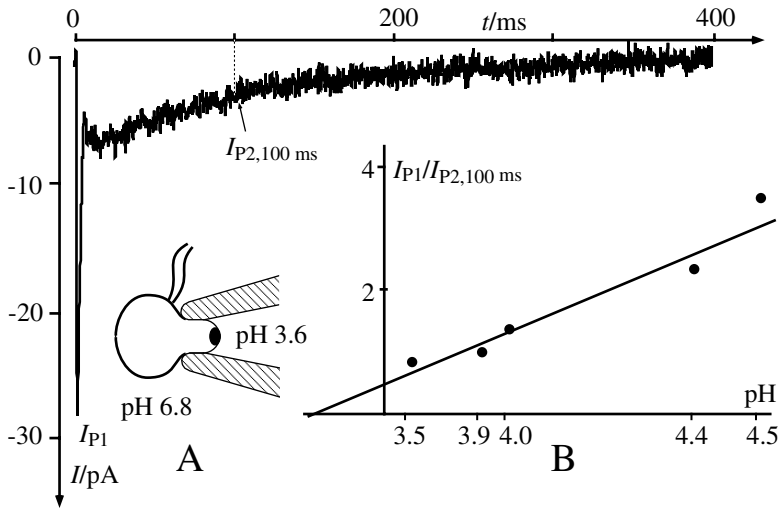

Fig. 4. Single recording of time courses of light-induced, rhodopsin-mediated currents from *C. reinhardtii* recorded in suction-pipette configuration with low external pH in the eye region; light flash (decay-time about 10 μsec): 625 μE m^{-2}; $[Ca^{2+}]_o = 0.1$, and $[K^+]_o = 1$ mM; Inset *A*: experimental configuration; Inset *B*: Lineweaver-Burk plot of typical stimulus-response-relationship of I_{P2} with respect to $[H^+]$ in external solution at the eye spot; data from Ehlenbeck et al., 2002.

$$p_i(t) = \sum_{j=L}^{O} (p_{ij} \cdot \exp(-k_j \cdot t)). \quad (5)$$

The amplitude coefficients p_{ij} (Table 3) can be derived from the system of differential equations (*not shown*) corresponding to the scheme (*4*) with the boundary conditions $p_L = Q/(Q_{1/2} + Q)$, and $p_{i>L} = 0$ for $t = 0$. The analytical solution of $p_i(t)$ applied here allows faster and more accurate calculations than iterative approaches.

Custom-tailored software has been written in Turbo Pascal 7.0 (Borland International INC) and is available on request.

Results

Experimental Data and Fit

For reference purposes, Fig. 4 illustrates the distinct response of I_P recorded at low pH in the pipette that is in contact with the eye spot (*see* inset *A*). Inset *B* of Fig. 4 shows that I_{P2} follows external $[H^+]$ at the eye spot by ordinary Michaelis-Menten kinetics. This relationship suggested that I_{P2} is carried by H^+. The evidence for Ca^{2+} being the predominant substrate of I_{P1} is given by Holland et al. (1996).

Figure 5 shows the ability of our two models to describe experimental data of I_{P1} and I_{P2} from *C. reinhardtii*. In this fit (solid line), all non-kinetic parameters have been kept constant at the values as listed in Table 1. And the four kinetic parameters, k_{LM}, k_{MN}, k_{NO}, and k_{OP} have been iteratively adjusted to the experimental data (dots) with starting values of 3000, 500, 100, and 20 sec^{-1} respectively. We notice that this fit is fair but not perfect. It is pointed out that in our approach the four amplitudes p_{ij} of the exponentials (Eq. 5) are not independent variables in addition to the four rate constants k_j; here, the amplitudes p_{ij} are strictly defined expressions of k_j (Table 3). So our approach uses four variables (four *k*s) only instead of the eight variables (four *k*s plus four amplitudes), which are generally required to describe four exponentials. Significantly better fits could be obtained, of course, if the amplitude coefficients and time constants had been fitted independently. However, such a formal treatment would be rather insignificant not only because of the considerably increased number of parameters to be fitted but mainly by the loss of the physical relationship $p_{ij} = f(k_j)$.

To avoid misinterpretations, the fitted current curve in Fig. 5 does not correspond directly to the time courses of the probabilities in Equation 5. In fact, these currents in Fig. 5 are the result of these probabilities *plus* the electrical properties of the complete circuit.

Application of the Kinetic Model for the Description of Current Records

Based on the constant and fitted parameters in Table 1, the intrinsic time courses of the four states *L*, *M*, *N*, and to *O* are shown in Fig. 6. These time courses are independent of the electrical properties of the two

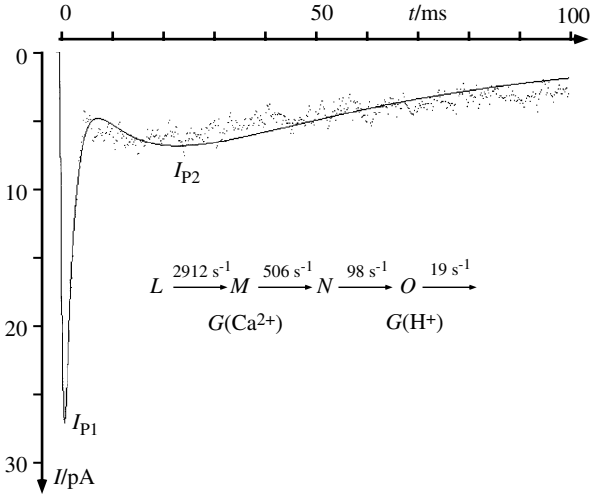

Fig. 5. Fit of the model (solid line) to one characteristic photocurrent recorded in the suction-pipette configuration; fitted kinetic parameters are presented in the inset; start values for fitted parameters k_{LM}, k_{MN}, k_{NO}, and k_{OP} are 3000, 500, 100, and 20 sec^{-1} respectively; fixed model parameters are also presented in Table 1; mean deviation of data from fit: 1.035 pA.

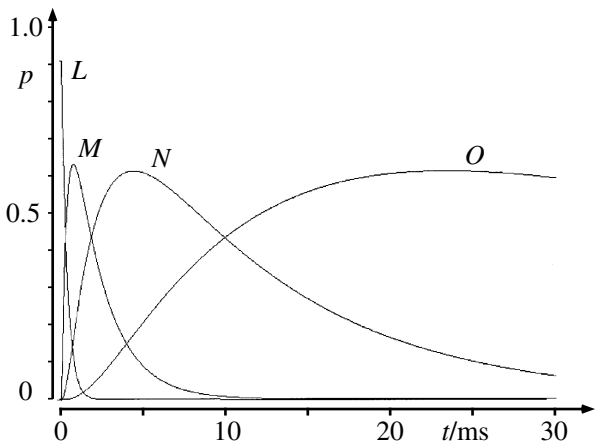

Fig. 6. Reconstructed time course of the occupancies of the states L, *M*, *N* and *O* after a 90% saturating flash of light.

models; they simply reflect the occupancies of the different states in the photocycle. In Fig. 6, *L* starts with a value of about 0.9, corresponding to a light flash of nearly saturating photon exposure.

The time courses of the 'true' Ca^{2+} currents and H^+ currents can be displayed and compared with the observed currents I_{P1} and I_{P2} by incorporating the electrical and the kinetic models and their identified parameters in Table 1.

Figure 7 shows that I_{P1} and I_{P2}, which are observed in the suction-pipette configuration, are only about 20% smaller than the calculated Ca^{2+} currents and H^+ currents, respectively. This result means that previous interpretations regarding the relative percentage of the currents that are actually recorded have been realistic.

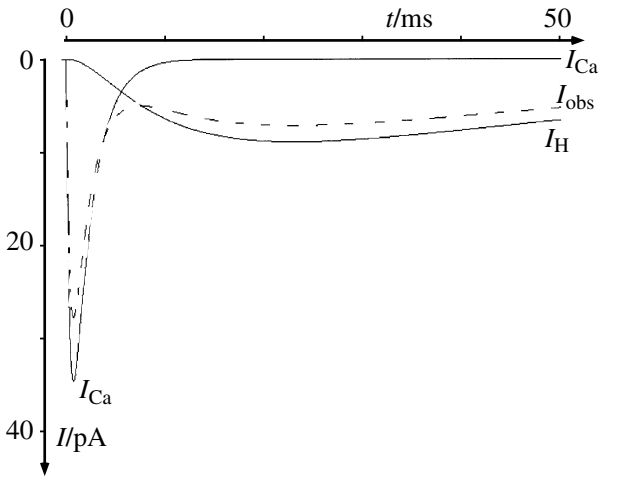

Fig. 7. Comparison of observed (*obs.*) and 'genuine', light-induced Ca^{2+} and H^+ currents through the eye of *C. reinhardtii*, inferred by model calculations with parameters as listed in Table 1.

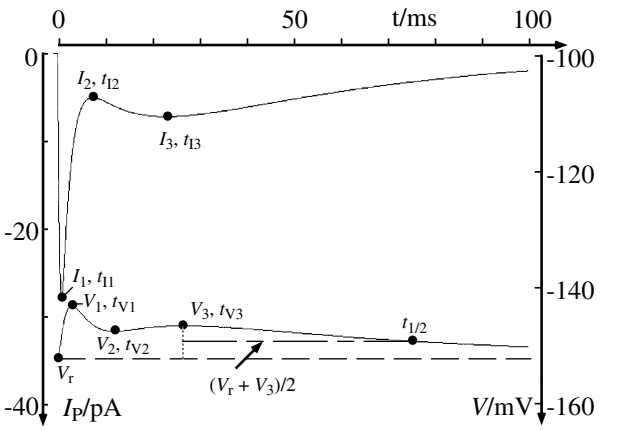

Fig. 8. Calculated time courses of the current (left ordinate), and of the inferred membrane voltage (right ordinate), with definitions of observable parameters used for the sensitivity analysis (Table 4).

Figure 8 displays the fitted time course of the observed current and the inferred time course of the membrane voltage, *V*. The *V* values are intermediate results (*V* at $I_p = I_b$) in the course of the calculations of the model currents as described by the paragraph Calculation of the Membrane Voltage above. The global result of Fig. 8 is that the changes in *V* upon a light flash are significant but not dramatic. However, larger *V* responses can be brought about by various modifications of the system parameters, e.g., if the cell surface were reduced to 50% and all other parameters would be constant, the light-induced *V* responses would be twice as large in the smaller cell. This relationship has already been suggested to hold for small vesicles that still contain the complete eye-

Table 4. Sensitivity analysis of the individual parameters of the two models

Model Parameter x	Change z* in observable parameter y													
	I_1 pA	t_{I1} msec	I_2 pA	t_{I2} msec	I_3 pA	t_{I3} msec	V_r mV	V_1 mV	t_{V1} msec	V_2 mV	t_{V2} msec	V_3 mV	t_{V3} msec	$t_{1/2}$ msec
Ref.	−26.4	0.75	−5.03	7.81	−7.16	23.4	−151	−142	3.12	−147	12.2	146	26.8	75.5
Background:														
A		–	0.28	–	0.34	–	–	−0.56	–	−0.27	–	−0.34	–	–
a_{pip}	−3.87	–	−2.49	–	−2.49	–	–	–	–	–	–	–	–	–
g_{Cl}	−0.07	–	−6.98	3.33	−8.66	–	−9.11	−9.3	–	−8.92	2.12	−8.77	−0.97	−0.34
$[Cl]_i$	0.07	–	−7.02	3.33	−8.7	–	−9.11	−9.3	–	−8.92	2.12	8.84	−0.97	−0.34
$[Cl]_o$	–	–	−0.18	–	0.04	–	–	–	–	–	–	–	–	–
E_p	–	–	0.04	–	−0.08		–	–	–	–	–	–	–	–
$I_{pu,mx}$	0.38	–	7.90	−3.34	9.97	–	10.0	10.65	–	10.1	−4.2	10.1	–	–
$[H^+]_i$	−1.21	–	8.00	−3.34	9.66	–	10.0	10.65	–	10.1	−4.2	10.1	–	–
$[H^+]_o$	0.02	–	7.6	−3.34	9.92	–	–	–	–	−0.2	−4.2	−0.34	–	–
c_m	–	–	−0.02	–	0.01	–	–	0.35	−7.68	–	2.20	0.07	0.97	0.69
Eye, non-kinetic														
Rht	10.0	–	9.7	–	9.61	–	–	–	–	−0.27	–	0.34	–	–
Light	0.8	–	0.8	–	0.81	–	–	–	–	–	–	–	–	–
$I_{ca,mx}$	9.93	–	1.85	−3.33	–	–	–	−0.56	–	–	–	–	–	–
g_H	–	–	7.6	−3.34	9.62	–	–	–	–	−0.2	–	−0.3	–	0.34
Eye, kinetic														
k_{LM}	0.38	−4.6	–	–	–	–	–	–	–	–	–	–	–	–
k_{MN}	−3.52	−2.3	−4.81	−6.67	–	−1.1	–	0.42	–	0.16	–	–	–	−0.40
k_{NO}	–	–	5.37	−3.34	2.22	−5.55	–	–	–	0.07	–	−6.07	–	–
k_{OP}	–	–	−0.05	–	−2.35	−3.33	–	–	–	–	2.12	0.14	–	−5.16

*Changes in the observable parameter y as a result of a 10% increase in a model parameter, x, are given in % change, $z = 100 \cdot dy/y$; if $(dy/dx)/y < 10^{-2}$, no numerical data (–).

spot after excision from the cells (Braun & Hegemann, 1999).

Observable parameters, defined and marked in Fig. 8, are used for the systematic sensitivity analysis in Table 4. This documentation describes the particular impacts of the individual model parameters (Table 1) x on the observable parameters y. Compared with $I(t)$, the time course $V(t)$ is smoother, and the maxima in V occur later than those in I. This delay reflects the RC-time, $r_m c_m$, of the membrane, where c_m is the membrane capacitance of about 10 mF m^{-2}. With $c_m = 0$, the times of the V peaks would coincide with those of the I peaks (not illustrated).

The numbers, z, in Table 4 are expressed as percent changes in y when x has been increased by 10%. For example, if the portion of the cell surface in the pipette, a_{pip} is increased by 10% from 0.20 to 0.22, the peak I_1 of the observed portion of the initial Ca^{2+} current will change by −3.87% (z-value) from its reference value −26.39 pA (also listed in Table 4) to −25.73 pA. This result reflects the finding that the recorded portion of the total eye current decreases as the portion of the cell outside the pipette (not containing the eye) increases (Holland et al., 1996), or that the observed current portions are smaller when the eye is together with the major part of the cell located outside the pipette.

The results of the sensitivity analysis of the models (Table 4) cannot be discussed in detail at this time. For such a purpose, virtually the entire literature on suction-pipette recordings should be discussed. Therefore, only some striking findings will be considered.

(*i*) One important result is that the time t_{I1} (0.75 msec) of the first current peak is insensitive to all model parameters listed, except k_{LM} and k_{MN}, of course, which determine the time of the peak directly. In particular, the insensitivity to the light intensity differs from the physiological observations, where the flash-to-peak time becomes shorter for increasing photon exposures (*see* below).

(*ii*) E_{Pu} has only a significant effect on the peak amplitude of the H^+ current, I_3. The vanishing effects of E_{Pu} on all the other observable parameters are due to the sigmoid $i(V)$ relationship of the pump, Eq. (1). Because of this sigmoidicity the pump behaves like a constant current source in the physiological V-range when the current becomes independent of V due to saturation. Accordingly, changes in this saturated pump current ($i_{Pu,mx}$), and the thermodynamic effect of $[H^+]_o$ itself have considerable impact on most observable parameters listed but not on the Ca^{2+} currents I_1, of course.

(*iii*) As mentioned already, c_m delays and smoothens $V(t)$ compared to $I(t)$, and has little effect on I itself. This finding is important for the interpretation of the recordings of transient, light-induced currents in the suction-pipette configuration. It means that these transients reflect genuine transmembrane currents that are not significantly biased by capacitive effects. This temporal order (I precedes V) differs from the situation in the animal eye, where the V-changes (of similar magnitude as here) cause major changes in currents through V-dependent channels.

(*iv*) As expected, the resting voltage, V_r, is independent of the properties of the eye.

(*v*) The effects of internal and external $[H^+]$ changes on I_2 and I_3 are somehow puzzling because effects of opposite signs might be expected for internal and external $[H^+]$. The situation is slightly complicated. In order to simplify the discussion, we focus only on the H^+ inward current I_3 through the eye here, and notice that I_2 behaves essentially in parallel. It is evident and numerically consistent with the results of the inset *B* in Fig. 4 that an increase of $[H^+]_o$ will cause a more or less proportional increase in I_3 by means of mass action, because I_3 represents an essentially unidirectional $[H^+]$ influx at highly negative V, where unidirectional $[H^+]$ efflux can be ignored. But why has $[H^+]_i$ such a similar effect? The answer is that the *direct* and opposite effect of $[H^+]_i$ on I_3 is small, and that the apparent effect of $[H^+]_i$ on I_3 is an *indirect* one, namely through the H^+ pump: According to Eq. 1, the pump current at V around −150 mV $\ll E_P$ will be V-independent but proportional to $[H^+]_i$ when the second term in the denominator vanishes. Hence, the pump current will increase with $[H^+]_i$ and will cause a correspondingly proportional increase of the voltage drop across g_m, which is the linear g_{Cl} in our approach. This effect of $[H^+]_i$ on the resting voltage V_r, as shown in Table 4, results in an increase of the electrical component of the driving force for $[H^+]$ inward current through the eye.

Flash-to-Peak Times

It is a flaw of the model, so far, that the flash-to-peak times are insensitive to the intensity of the light stimulus, whereas experimental data show an acceleration with increasing intensities. For the low-intensity range, this feature has been explained by superposition of the effects of the two systems *a* and *b* (Ehlenbeck et al., 2002): compared with system *b*, system *a* is slower, and saturates at about 100 times smaller intensities, with 10 times smaller amplitudes. However, this mechanism does not account for the high-intensity range when system *a* is invariant because of saturation. But intensity-dependent flash-to-peak times are evident in this range as well.

Based on the notion of V-sensitive kinetics of rhodopsin (Nagel et al., 1998, Geibel et al., 2001) our working hypothesis for these kinetics in the high-intensity range is that the rate constant k_{MN} depends on

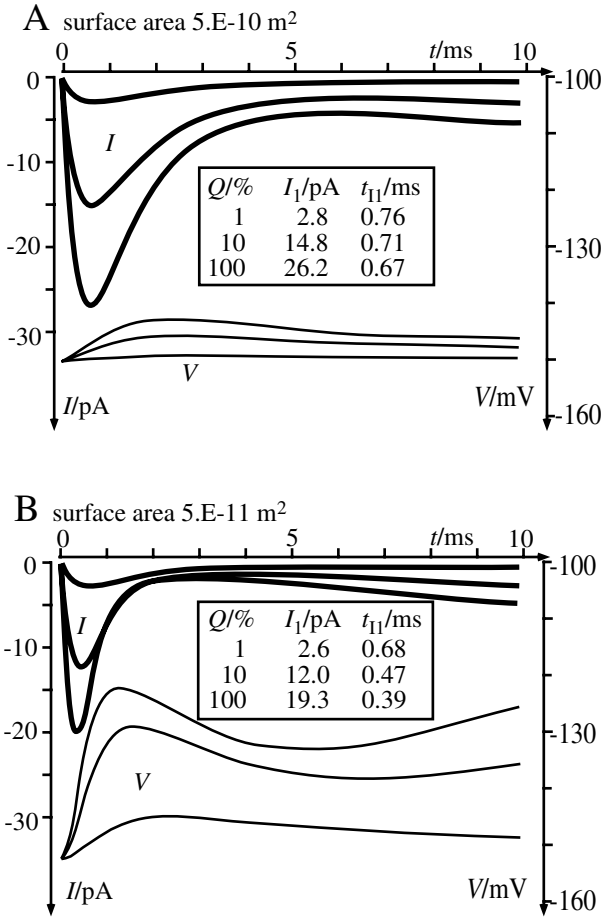

Fig. 9. Changes in I and V upon light flashes in model with V-dependent k_{MN}. Three different intensities and coordinates of resulting current peaks are listed in insets. Unless specified, all parameters as listed in Table 1. (*A*) Normal cell with typical surface area. (*B*) Small cell with ten times less surface area, equivalent to vesicles used by Braun and Hegemann (1999). Main result: model configuration for shortening of flash-to-peak times by increasing light intensities.

V. As a first approach, we express this dependency in the form

$$k_{MN} = k^0_{MN} e^u, \tag{6}$$

where k^0_{MN} is k_{MN} at $V = 0$. With k_{MN} of 506 sec^{-1} and $V = -151$ mV from the fit in Fig. 5, k^0_{MN} can be calculated by $k^0_{MN} = k_{MN} e^{-u}$ to be about $2 \cdot 10^5$ sec^{-1}. The hypothesis assumes that the decay of the Ca^{2+}-conducting state M to the nonconducting state N becomes faster when V becomes more positive. So the maximum of I_1 will be lower and earlier. The magnitude of this effect will increase with the positive voltage change. We know two parameters with major effects on the change in V upon light flashes, the surface area of the entire cell, and the light intensity.

Model calculations using the standard configuration (Table 1), and Eq. 6 are illustrated in Fig. 9 for various light intensities, and for cells with various surface areas. The results in Fig. 9, numerically specified by the insets, show, indeed, that after implementation of Eq. 6, (*i*) the flash-to-peak times decrease with increasing intensity, (*ii*) this effect vanishes at low intensities, and (*iii*) this effect is much larger in small cells.

Discussion

In general, the combination of an electric equivalent circuit for the electrophysiological suction-pipette configuration and a reaction cycle of light-induced excitation and relaxations of rhodopsin allows a first, quantitative interpretation of rhodopsin-mediated current transients recorded from the eye of *C. reinhardtii* in response to stimulation with short light flashes.

The combination of the two models enables the description of measured time courses of I_{P1b} and I_{P2b} for a given photon exposure fairly well. In addition, it predicts for the first time the sensitivity of the photocurrents to intrinsic and extrinsic parameters. For example, the model provides an estimate for the time course of the membrane voltage, suggesting that the small voltage changes are not responsible for the refractory period of the photocurrents observed in double-flash experiments (Govorunova & Hegemann, 1997; Govorunova et al., 2001). The model in its basic form is only a coarse approach, of course. Accounting for more realistic scenarios would require appropriate extensions of the model.

Flash-to-Peak Times

The two models in their basic version, without system *a*, do not account for changes of the flash-to-peak time at high flash energies between 1 and 100% rhodopsin excitation (Table 4). In order to explain the experimental observations, which seem to be inconsistent with the theory so far, extensions of the theory are necessary. To achieve this consistency in the low-intensity range, we simply have to add the currents through the high-affinity system *a*, as proposed previously (Ehlenbeck et al., 2002) because combining the slow, low light-saturating component *a* with the fast, high light-saturating component *b* to different ratios, results in intermediate temporal locations of the peak, earlier at higher intensities, and later at lower intensities. However, the kinetics still changes between 2 and 100% light saturation when the *a* component has already been saturated (Fig. 7*b* in Ehlenbeck et al., 2002). Thus, alternative mechanisms have to be discussed, e.g., that the photocycle of the Rh_b in Fig. 3 has a voltage-sensitive component, as suggested by Harz et al. (1992).

This mechanism of voltage-dependent kinetics of the photocycle has specifically been implemented into

the basic model combination by Eq. 6. The results of corresponding calculations in Fig. 9 do satisfy the experimental observations of kinetic acceleration in the high-intensity range. In particular, these model calculations with a V-dependent step, k_{MN} (V), in the photocycle simulate the following two experimental observations. First, shorter flash-to-peak times and faster kinetics have been found upon an increase of external [K^+] (Nonnengäßer et al. 1996), which depolarizes biomembranes in general, and specifically in *C. reinhardtii* as well (Malhotra & Glass, 1995). Second, Braun and Hegemann (1999) measured light-induced I-changes using the eye-in-pipette configuration with progressively reduced cell bodies. They observed, the smaller the body, the earlier and smaller the current peak. The latter observations specifically confirm the theoretical results in Fig. 9*B* compared to Fig. 9*A*.

Which Types of Rhodopsin are Involved?

For the sake of simplicity, only one type of rhodopsin has been treated in this study. The two components of light-induced, rhodopsin-mediated currents in the eye of *C. reinhardtii* at neutral and at acidic external pH (I_{P1b} and I_{P2b} in Ehlenbeck et al., 2002), correspond to a Ca^{2+} conductance and a H^+ conductance, which are represented by two out of 7 distinct states of the rhodopsin photocycle.

The nature of the essential chromophore for phototaxis in *C. reinhardtii* is *all-trans*, isomerizing to *13-cis* in the light, as identified by in vivo characterization of the retinal binding site via reconstitution of blind mutants with retinal and retinal-analog compounds and subsequent analysis of the photocurrents or the behavior (reviewed by Sineshchekov and Govorunova, 2001). After reducing the type-2 opsins of the *C. reinhardtii* eye (chlamyopsin-1 and -2) by application of an antisense approach, it was shown that these are not the photoreceptors that mediate photocurrents and behavioral responses (Fuhrmann et al., 2001). Thus, the only photoreceptor candidate in sight is the archaean-type rhodopsin chlamyrhodopsin-3 (Hegemann, Fuhrmann & Kateriya, 2001). In this rhodopsin the amino acids that define the proton-conducting network in bacteriorhodopsin (Luecke et al., 1999) are highly conserved. In fact, chlamyrhodopsin-3, expressed in *Xenopus* oocytes, catalyzes light-induced, passive H^+ currents (Nagel et al., 2002). In conclusion, the properties of system *b* that are modeled here, in particular the numerical details (Table 1) of its photocycle with an intrinsic H^+ conducting intermediate M, can be attributed to channelrhodopsin-1 (chlamyrhodopsin-3). It should be kept in mind that this study follows the commandment to use the simplest model to describe the available data. More experimental results may require, of course, substantial modifications of the model by additional reactants.

We thank Drs. Carl M. Boyd, Elena Govorunova, Ulrike Homann, and Gerhard Thiel for critical reading of the manuscript. This work was supported by grants of the Deutsche Forschungsgemeinschaft (SFB 521 Pr. 91017) to P.H. and of the Volkswagen-Stiftung (1/76841) to D.G.

References

Beckmann, M., Hegemann, P. 1991. *In vitro* identification of rhodopsin in the green alga *Chlamydomonas*. *Biochemistry* **30:** 3692–3697

Braun F.J., Hegemann, P. 1999. Two independent photoreceptor currents in the spheroidal alga *Volvox carteri*. *Biophys. J.* **76:**1668–1678

Calenberg, M., Brohsonn, U., Zedlacher, M., Kreimer, G. 1998. Light- and Ca^{2+}-modulated heterotrimeric GTPases in the eyespot apparatus of a flagellate green alga. *Plant Cell* **10:**91–103

Ehlenbeck S., Gradmann, D., Braun F.J., Hegemann, P. 2002. Light-induced H^+-conductances in the eye of the green alga *Chlamydomonas reinhardtii*. *Biophys. J.* **282:**740–751

Fuhrmann, M., Govorunova, E.G., Rank S., Hegemann, P. 2001. The dominant retinal protein of the *C. reinhardtii* eye is not the photoreceptor for phototaxis. *J. Cell Sci.* **114:**3857–3862

Geibel, S., Friedrich, T., Ormos, P., Wood, P., Nagel, G., Bamberg, E. 2001. The voltage depending proton pumping in Bacteriorhodopsin is characterized by optoelectric behavior. *Biophys. J.* **81:**2059–2068

Govorunova, E.G., Hegemann, P. 1997. Desensitisation and dark recovery of the photoreceptor current in *Chlamydomonas reinhardtii*. *Plant Physiol.* **115:**633–642

Govorunova, E.G., Sineshchekov, O.A., Gärtner W., Chunaev, A.S., Hegemann, P. 2001. Photoreceptor currents and photoorientation in *Chlamydomonas* mediated by 9-demethyl-chlamyrhodopsin. *Biophys. J.* **81:**2897–2907

Hansen, U.-P., Gradmann, D., Sanders, D., Slayman, C.L. 1981. Interpretation of current-voltage relationships for "active" ion transport systems: I. Steady-state reaction-kinetic analysis of Class-I mechanisms. *J. Membrane Biol.* **63:**165–190

Harz, H., Hegemann, P. 1991. Rhodopsin-regulated calcium currents in *Chlamydomonas*. *Nature* **351:**489–491

Harz, H., Nonnengäßer, C., Hegemann, P. 1992. The photoreceptor current of the green alga *Chlamydomonas*. *Phil. Trans. R. Soc. Lond. B.* **338:**39–52

Hegemann, P., Fuhrmann, M., Kateriya, S. 2001. Algal Sensory Photoreceptors. *J. Phycol.* **37:**668–676

Holland, E.M., Braun, F.-J., Nonnengäßer, C., Harz, H., Hegemann, P. 1996. The nature of rhodopsin triggered photocurrents in *Chlamydomonas*. I. Kinetics and influence of divalent ions. *Biophys. J.* **70:**924–931

Litvin, F.F., Sineshchekov, O.A., Sineshchekov, V.A. 1978. Photoreceptor electric potential in the phototaxis of the alga *Haematococcus pluvialis*. *Nature Lond.* **271:**476–478

Luecke, H., Richter, H.T., Lanyi, J.K. 1998. Proton transfer pathways in bacteriorhodopsin at 2.3 Angstrom resolution. *Science* **280:**1934–1973

Malhotra, B., Glass, A.D.M. 1995. Potassium Fluxes in *Chlamydomonas reinhardtii*. *Plant* **108:**1527–1536

Nagel, G.B., Kelety, B., Mockel, B., Büldt, G., Bamberg, E. 1998. Voltage dependence of proton pumping by bacteriorhodopsin is regulated by the voltage-sensitive ratio of M1 and M2. *Biophys. J.* **74:**403–412

Nagel, G., Ollig, D., Fuhrmann, M., Kateriya, S., Musti, A.M., Bamberg, E., Hegemann, P. Channelrhodopsin-1: a light-gated proton channel in green algae. *Science*, **1296:** 2395–2398

Nichols, K.M., Rikmenspoel, R. 1978. Control of flagellar motion in *Chlamydomonas* and *Euglena* by mechanical microinjection of Mg^{2+} and Ca^{2+} and by electrical current injection. *J. Cell Sci.* **29:**233–247

Nonnengäßer, C., Holland, E.M., Harz, H., Hegemann, P. 1996. The nature of rhodopsin-triggered photocurrents in *Chlamydomonas*. II: Influence of monovalent ions. *Biophys. J.* **70:**932–938

Sineshchekov, O.A., Litvin, F.F., Keszethely, L. 1990. Two components of the photoreceptor potential in phototaxis of the flagellated green alga *Haematococcus pluvialis*. *Biophys. J.* **57:**33–39

Sineshchekov, O.A., Govorunova, E.G. 2001. Electrical events in photomovement of green flagellate algae. In: Photomovement. eds: D.-P. Häder and M. Lebert, pp. 245–280. Comprehensive Series in Photosciences Vol. 1. Elsevier, North-Holland

Zacks, D.N., Derguini, F., Nakanishi, K., Spudich, J.L. 1993. Comparative study of phototactic and photophobic receptor chromophore properties in *Chlamydomonas reinhardtii*. *Biophys. J.* **65:**508–518